NJC

Synthesis of dual pH and temperature responsive star triblock copolymer based on β-cyclodextrins for controlled intracellular doxorubicin delivery release

Journal:	*New Journal of Chemistry*
Manuscript ID	NJ-ART-04-2016-001360.R1
Article Type:	Paper
Date Submitted by the Author:	25-Jun-2016

Complete List of Authors:	Lu, Beibei; School of Chemistry & Chemical Engineering, Shihezi University Li, Lei; School of Chemistry & Chemical Engineering, Shihezi University Wu, Jianning; School of Chemistry & Chemical Engineering, Shihezi University Shihezi, CN Wei, Lulu; shihezi university Hou, Jun; epartment of immunology, Shihezi University School of Medicine/Department of Pathology and Key Laboratories for Xinjiang Endemic and Ethnic Diseases Liu, Zhiyong; School of Chemistry & Chemical Engineering, Shihezi University, Guo, Xuhong; East China University of Science and Technology, School of Chemical Engineering

Journal Name

ARTICLE

Synthesis of dual pH and temperature responsive star triblock copolymer based on β-cyclodextrins for controlled intracellular doxorubicin delivery release

Received 00th January 20xx,
Accepted 00th January 20xx

DOI: 10.1039/x0xx00000x

www.rsc.org/

Beibei Lu [a], Lei Li[a], Jianning Wu[a], Lulu Wei[a], Jun Hou[b], Zhiyong Liu*[a], Xuhong Guo[a,c]

Well-defined dual pH and temperature responsive triblock star-shaped amphiphilic copolymer of β-Cyclodextrin-g-poly(2-(Dimethylamino)ethylmethacrylate-*b*-N-Isopropylacrylamide-*b*-2- Hydroxy ethyl methacrylate) (β-CD-*g*-(PDMAEMA-*b*-PNIPAM-*b*-PHEMA)) were synthesized by combination of reversible addition-fragmentation chain transfer (RAFT). The chemical structures and compositions of these copolymers have been characterized by fourier transforms infrared spectroscopy (FTIR), nuclear magnetic resonance (^{1}H NMR), and gel permeation chromatography (GPC) measurements. Subsequently, the obtained triblock copolymers could self-assemble into micelles in aqueous solution owing to the amphiphilic property resulting from the hydrophobic β-CD core and the hydrophilic PHEMA, PNIPAM, and PDMAEMA segments, which were investigated by dynamic light scattering (DLS) and transmission electron microscopy (TEM). The triblock copolymer nanoparticles exhibited two separate lower critical solution temperatures (LCST) and these triblock copolymers in aqueous solutions were investigated at different pH value of 5.0 and 7.4 as doxorubicin delivery for controlled release. Polymeric micelles exhibited pH controlled-release performance. The investigation of doxorubicin release from the micelles indicated that the release rate of the drug could be effectively controlled by altering pH, and sealed DOX in neutral surroundings (blood circulation or extracellular matrix) and triggered DOX release in acidic surroundings (intracellular endosomes). CCK-8 assays and confocal laser scanning microscopy (CLSM) against HeLa cells indicated that the polymeric micelles themselves had no associated cytotoxicity and possessed good biodegradability and biocompatibility and identified the location of the DOX in HeLa cells. While DOX-loaded micelles possessed high cytotoxicity to HeLa cells and exhibited inhibition of the proliferation of HeLa cells. Hence, this kind of biodegradable, biocompatible and stimuli-responsive copolymers could be served as a promising material for drug delivery.

1. Introduction

In recent years, cancers remained the most disastrous diseases worldwide. However, chemotherapy was usually restricted by the severe cytotoxicity of anticancer drugs to normal tissues and cells.[1] For this purpose, many researchers had paid much attention to various drug formulations micelle to reduce the side effects and improve the therapeutic efficacy of anticancer drugs.[2] Among them, biocompatible and biodegradable amphiphilic polymeric micelles have become some of the most promising carriers especially for poorly water-soluble anticancer drugs, such as the doxorubicin (DOX).[3] This strategy could not only overcome some limitations associated with small molecule chemotherapeutic drugs, but greatly improve drug bioavailability via either passive targeting by the enhanced permeability and retention (EPR) effect[4, 5] or active targeting by introducing some specific tumor-homing ligands.[6]

Star-shaped block copolymers have attracted extensive interests during the past decade due to the potential applications as “smart materials”, especially biomedical applications.[7-10] And their self-assembled structures that were able to respond to changes in their environment such as variations in temperature[11-14], pH[8, 15, 16] or light.[17] Star

[a]School of Chemistry & Chemical Engineering, Shihezi University/Key Laboratory of Materials-Oriented Chemical Engineering of Xinjiang Uygur Autonomous Region/Engineering Research Center of Materials-Oriented Chemical Engineering of Xinjiang Bingtuan, Shihezi 832003, P. R. China.
[b]Department of immunology, Shihezi University School of Medicine/Department of Pathology and Key Laboratories for Xinjiang Endemic and Ethnic Diseases, Shihezi University School of Medicine, Xinjiang 832003, China.
[c]State Key Laboratory of Chemical Engineering, East China University of Science and Technology, Shanghai 200237, P. R. China.
DOI: 10.1039/x0xx00000x
*Correspondence to: Zhiyong Liu (E-mail: lzyongclin@sina.com)

polymers were first realized using ionic polymerization technique[18]. Following polymerization-induced self-assembly, controlled/living radical polymerization such as reversible addition-fragmentation chain transfer (RAFT)[19-21], nitroxide-mediated radical polymerization (NMRP), ring-opening polymerization (ROP)[22], Click chemistry[23], and atom transfer radical polymerization (ATRP)[24, 25] could be highlighted in particular. However, this method has its limitations according to the small range of applicable monomers. With the development of controlled radical polymerization (CRP) in the mid-1990s, a new and powerful tool was found to create polymers with complex architectures. Beside, RAFT the synthetic procedures providing well-defined star macromolecules could be separated into three different categories: the "arm-first" approach[26] contains the cross-linking of linear arm precursors with a cross-linking agent; the "coupling-onto" approach comprises the grafting of linear arm precursors onto a well-defined multifunctional core; and the "core-first" approach[27] requires the use of a multifunctional initiator (core) to initiate the growth of the polymer chains. What was more, the heterogeneous RAFT polymerization provides additional benefits such as use of the low viscosities, environmental friendly solvents water and alcohol, fast heat dissipation and fast polymerization rates due to the radical compartmentalization effect.

As we all know, cyclodextrins (CDs) were a range of cyclic oligosaccharides that comprise several glucopyranose linked by *a*-(1, 4) glycosidic bonds. Because of steric effect, *a*-, β- and *r*-CD containing 6, 7 or 8 D-glucose units could be produced using genetic engineering techniques.[28] Their unique three-dimensional architecture with hydrophobic inner cavity endows them with the attracting character to form host-guest inclusion via hydrophobic and Van der Waals effect, or other specific interactions. Taking strengths of this point, CDs have been widely used as drug carriers to enhance the solubility, stability, and thus bioavailability of drug, achieve sustained drug release, as well as made the oily drug solidification.[29-31] β-CD was not only a suitable backbone for designing functional branched copolymers, but a suitable hydrophilic component with inclusive ability to generate amphiphiles. However, up to now reported on β-CD-based synthetic macro-RAFT agent initiator of literature also was less.

Recently, polymeric micelles as promising nanosized antitumor drug carriers were being extensively studied. For instances, Yuan *et al* [32] synthesised of this star copolymer initiates with β-CD core, from which sequential polymerization of a temperature-responsive poly(N-isopropylacrylamide) (PNIPAM) block and a hydrophilic poly (N, N-dimethylacrylamide) (PDMA) block as asymmetric arms (named β-CD-*g*-(PNIPAM-*b*-PDMA)$_3$) was performed via RAFT protocol. Charleux *et al*. [33] reported the preparation of crosslinked poly (N, N-diethylacrylamide) nanogels through aqueous dispersion RAFT polymerization in the presence of the amphiphilic poly (ethylene oxide)-*b*-poly (N, N-dimethylacrylamide) macro-RAFT agent. It was founded that the size and stability of the resultant nanogels were dependent strongly on the chain length of the macro-RAFT agent monomer for aqueous dispersion RAFT polymerization. Zhang *et al* [34] prepared doubly thermo-responsive triblock copolymer nanoparticles of poly(N-isopropylacrylamide)-block-polyN, N-(dimethylamino) ethyl methacrylate]-block-polystyrene (PNIPAM-*b*-PDMAEMA-*b*-PS) and PDMAEMA-*b*-PNIPAM-*b*-PS containing two thermo-responsive blocks of poly(N-isopropylacrylamide) (PNIPAM) and poly[N, N-(dimethylamino) ethyl methacrylate] (PDMAEMA) by a macro-RAFT agent mediated dispersion polymerization through a polymerization-induced self-assembly. As known, N-isopropylacrylamide (NIPAM) was a water-soluble monomer, while the polymer, poly(N-isopropylacrylamide) (PNIPAM), was a thermo-responsive polymer which had a lower critical solution temperature (LCST) of 32^{o}C. Zhang *et al* [35] synthesized a novel cyclodextrin-containing pH-responsive star polymer by atom transfer radical polymerization using the arm-first approach. Copolymerization of a mixture of mono- and multi-methacrylate substituted cyclodextrin and 2-(dimethylamino) ethyl methacrylate initiated by poly(ethylene glycol) macroinitiator produced a core cross-linked star polymer. In vitro experiments demonstrated that the DOX-loaded nanoparticles could release their payload in response to the endosomal-pH after being internalized by HeLa cell via endocytosis.

In order to further improve delivery efficiency, a promising method has been developed aiming at achieving synergistic effects by the combination of two or more therapeutic approaches with different mechanisms. For instance, the polymeric micelles self-assembled from amphiphilic block copolymers, which have hydrophobic core to encapsulate some poorly water-soluble drugs and hydrophilic shell to stabilize micelles, hold enormous potential to increase the drug efficacy by means of reducing toxicity, improving the water solubility, prolong circulation time in blood and the enhanced uptake by tumors.[36, 37] Therefore, how to prepare a good water-soluble and biocompatible polymeric with stimuli-responsive linker and low cytotoxicity by means of efficient synthesis methods was still a fatal issue.

In this study, we well synthesized a dual pH and temperature responsive β-CD-*g*-(PHEMA-*b*-PNIPAM-*b*-PDMAEMA)$_3$ amphiphilic triblock copolymers via RAFT with β-CD-(xanthate) as initiator, HEMA, NIPAM, and DMAEMA as monomers. These dual pH and temperature-responsive star-shaped triblock copolymers showed critical phase transition temperature in water. The star-shaped triblock copolymers could self-assemble into spherical nano-micelles in water, and the tunable thermo-sensitive properties, which the morphology of these micelles was observed by UV-vis, DLS and TEM. The self-assembly and pH responsive properties of the copolymer in water were investigated. The release of DOX from DOX-loaded micelles could be effectively controlled by altering the pH value. At the same time, the cellular uptake and cytotoxicity test to HeLa cells were also performed. Hence, such amphiphilic copolymer could be a potential candidate for stimuli-responsive drug delivery vector.

2. Experimental

2.1. Materials

β-Cyclodextrin (β-CD, >98%, and purified by recrystallization from water twice prior to use), carbon disulfide (CS_2), Methyl 2-bromobutyrate were purchased from Aladdin. N-isopropylacrylamide (NIPAM, Acros) was recrystallized twice from toluene and cyclohexane (3:2). 2, 2-Azobis(isobutyronitrile) (AIBN, was purchased from Sigma-Aldrich). Hydroxyethyl methacrylate (HEMA, Aldrich) and 2-(Dimethylamino)ethyl methacrylate (DMAEMA 98%, Sigma-Aldrich) was filtered over aluminum oxide to remove the inhibitor (MEHQ) before being polymerized. Doxorubicin hydrochloride (DOX·HCl) was purchased from Beijing Hua Feng United Technology Co. Ltd. Dimethylformamide (DMF) and triethylamine (TEA) were dried by refluxing over CaH_2 and distilled just before use. HeLa cells (Institute of cells, CAS, Shanghai) were used as received, Cell Counting Kit-8 (CCK-8, Shanghai, Beyotime Biotechnology), Dulbecco's modified Eagle medium (DMEM), fetal bovine serum (FBS), pancreatic enzymes were obtained from biological industries. 4% Paraformaldehyde, 4', 6-Diamidino-2-phenylindole (DAPI) and TritonX-100 were purchased from Solarbio.

2.2. Characterization

^{1}H NMR data were obtained by Nuclear Magnetic Resonance Spectroscopy (NMR) using a BrukerDMX-500 NMR spectrometer with DMSO-d_6 as solvent. Fourier Transform Infrared Spectroscopy (FTIR) analysis was measured by Nicolet Avatar 360 using KBr pellets. The molecular weight and molecular weight distribution of copolymers were measured by Gel Permeation Chromatography (GPC) using a Viscotek TDA 302 gel permeation chromatograph and DMF was used as eluent. The transmittances of copolymers aqueous solutions at various temperatures were measured at a wavelength of 500 nm on a UV-visible spectrophotometer (UV-vis). The LCST value of the copolymer solution was defined as the temperature producing a 50% decrease in transmittance. Dynamic Light Scattering (DLS) measurements were performed by a BECKMAN COULTER Delasa Nano C particle analyzer at a fixed angle of 165°. Before the light scattering measurements, the sample solutions were filtered three times by using Millipore Teflon (Nylon) filters with a pore size of 0.45 μm. All measurements were repeated three times, and the average results were accepted as the final hydrodynamic diameter (D_h) and zeta potential (mV). Samples for transmission electron microscopy (TEM) images were taken on an H-600 transmission electron microscope (Hitachi, Japan) operating at 120 kV. Confocal Laser Scanning Microscopy images (Zeiss CLSM510) was operated.

2.3. Synthesis of β-CD-*g*-(PHEMA-*b*-PNIPAM-*b*-PDMAEMA)$_3$ with star amphiphilic triblock copolymers via RAFT

2.3.1 Synthesis of β-CD-(xanthate)$_3$ chain transfer agent

A typical procedure employed for the synthesis of β-CD (xanthate)$_3$ with a target degree of substitution of 3 was as follows[38]. The β-CD (6.00 g, 5.29 mmol) was dissolved in 50 mL 20 wt% NaOH aqueous solution. CS_2 (1.2 mL, 19.8 mmol) was added dropwise via constant pressure funnel over 0.5 h. The solution turned orange gradually. After further stirring for 4 h at room temperature, the solution was precipitated in excess ethanol. Then the crude product was dissolved in water and precipitated in ethanol three times. The product was dried under vacuum at 50^{o}C , The intermediate product was obtained as β-CD-(XNa)$_3$。 Then, β-CD-(XNa)$_3$ (4.00 g) was dissolved in 30 mL distilled water. Methyl 2-bromobutyrate (2.6 mL) was added dropwise via constant pressure funnel over 0.5 h and the reaction mixture kept stirring at 35^{o}C until light yellow precipitate appeared. The suspension was filtrated and washed with water and diethyl ether repeatedly. The product was obtained β-CD-(xanthate)$_3$ and β-CD-(xanthate)$_3$ as the chain transfer agent were successfully synthesized. Following similar procedures, β-CD-xanthate with a target substitution degree of 1 was also synthesized by adjusting the β-CD/CS_2 molar ratio.

2.3.2 Synthesis of β-CD-*g*-(PHEMA-*b*-PNIPAM)$_3$ by RAFT

β-CD-g-(xanthate)$_3$ (0.1 g, 0.035 mmol), HEMA (1.36 g, 10.5 mmol), NIPAM (1.00 g, 8.80 mmol), AIBN (1.6 mg, 0.01 mmol) in 25 mL of DMF in a 100 mL flask quipped with a magnetic stirring bar was degassed with three freeze-evacuate-thaw cycles. Then, the polymerization was performed at 70^{o}C for 24 h. After the polymerization was cooled to room temperature, and the resultant mixture was precipitated into an excess diethyl ether. The precipitate was dissolved in DMF and then precipitated again into an excess of diethyl ether. The above dissolution precipitation cycle was repeated three times. The final product was dried in vacuum at 50^{o}C.

2.3.3 Synthesis of β-CD-*g*-(PHEMA-*b*-PNIPAM-*b*-PDMAEMA)$_3$ by RAFT

The polymer synthesis starts from the synthesis of a β-CD-based chain transfer agent (CTA), from which the β-CD core star-shaped copolymer β-CD-*g*-(PHEMA-*b*-PNIPAM-*b*-PDMAEMA)$_3$ was obtained through the growth of PHEMA-*b*-PNIPAM-*b*-PDMAEMA arms by reversible addition-fragmentation chain transfer (RAFT) radical polymerization method (Scheme 1).

β-CD-*g*-(PHEMA-*b*-PNIPAM)$_3$ (0.1 g, 0.0028 mmol), DMAEMA (1.00 g, 6.36 mmol), AIBN (1.6 mg, 0.01 mmol), and 25 mL DMF were added into a 100 mL round-bottom flask, followed by three freeze-vacuum-thaw cycles. The flask was immersed into an oil bath at 70^{o}C with magnetic stirring. After reaction for 24 h, and the resultant mixture were precipitated into an excess diethyl ether. The precipitate was dissolved in DMF and then precipitated again into an excess of diethyl ether. The above dissolution precipitation cycle was repeated three times. The final product was dried in vacuum at 50^{o}C。 Table 1 summarizes structural parameters of β-CD-*g*-(PHEMA-*b*-PNIPAM)p and β-CD-*g*-(PHEMA-*b*-PNIPAM-*b*-PDMAEMA)p copolymers synthesized in this work.

2.4 Self-assembly of β-CD-*g*-(PHEMA-*b*-PNIPAM-*b*-PDMAEMA)$_p$ in aqueous solution

Samples for UV-vis, DLS, and TEM were prepared as follows: β-CD-*g*-(PHEMA-*b*-PNIPAM-*b*-PDMAEMA)$_3$ (20 mg) was dissolved in 2 mL DMF and subsequently, deionized water (2 mL) was added dropwise from an additional funnel over a period of 0.5 h. After 4 h quick stirring, 8 mL water was added to quench the micellar

assembly. Then used dialysis (molecular weight cut-off: 3500 Da) against distilled water for 72 h, and micelles with different concentrations could be obtained by diluting with distilled water. During this dialysis process, the triblock copolymers self-assembled into micelles with β-CD core and star-shaped PHEMA-*b*-PNIPAM-*b*-PDMAEMA shells, and were named PHND1 and PHND3.

2.5 DOX encapsulation and release studies

100 mg of PHND1/PHND3 and 10 mg of DOX·HCl, were dissolved in 2 mL of DMF separately and the two solutions were mixed in a vial and stirred for 0.5 h, then, a 3-fold excess of TEA in 2 mL DMF overnight to obtain DOX base. Then the mixture was added dropwise using a syringe pump to water (30 mL) under high-speed stirring. The DOX-containing suspension was then equilibrated under stirring at room temperature for 4 h, followed by thorough dialysis (molecular weight cut-off: 3500 Da) against deionized water for 48 h to remove unloaded DOX, and it were named D-PHND1 and D-PHND3.

The DOX loading content (LC) and entrapment efficiency (EE) were determined by UV-vis spectrophotometry at 480 nm. To determine the drug loading level, a small portion of DOX-loaded micelles was withdrawn and diluted with DMF to a volume ratio of DMF/H_2O=9/1. The amount of DOX encapsulated was quantitatively determined by a UV-vis spectrophotometer and the calibration curve used for drug loading characterization was established by the intensity of DOX with different concentrations in DMF/H_2O=9/1 (v/v) solutions. The DLC was defined as the weight ratio of entrapped DOX to that of the DOX-loaded micelles. The DLE of DOX was obtained as the weight ratio between DOX incorporated in assembled micelles and that used in fabrication.

$$\mathrm{DLC(wt\%)} = \frac{\text{weight of loaded drug}}{\text{weight of polymer}} \times 100 \quad (1)$$

$$\mathrm{DLE(wt\%)} = \frac{\text{weight of loaded drug}}{\text{weight of drug in feed}} \times 100 \quad (2)$$

The in vitro DOX release profiles from the PHND1/PHND3 assembled micelles were evaluated using buffers (PB, 10 mM) solution with pH values 5.0 and 7.4. In each experiment, 4 mL of DOX-loaded nanoparticle solution was transferred into a dialysis bag (molecular weight cut-off: 3500 Da), and immersed into a tube containing 60 mL of buffer solution and shaken (200 rpm) at 37°C. At specified time intervals 4 mL (V_e) samples were taken and an equal volume of fresh buffer added to maintain the total volume. The concentration of DOX in different samples was analyzed by UV-vis spectrophotometry at 480 nm. The cumulative percent drug release (E_r) was calculated using

$$\mathrm{E_r(\%)} = \frac{\mathrm{V_e}\sum_1^{n-1}\mathrm{C_i} + \mathrm{V_0C_n}}{\mathrm{m_{DOX}}} \times 100 \quad (3)$$

where m_{DOX} represents the amount of DOX in the micelle, V_0 was the volume of the release medium (V_0=50 mL), and Cn represents the concentration of DOX in the nth sample. The in vitro release experiments were carried out in triplicate at each pH and temperature and the reported results were the average values with standard deviations.

2.6 Cytotoxicity test

The cytotoxic effects of polymers, free DOX or DOX-loaded β-CD-*g*-(PDMAEMA-*b*-PNIPAM-*b*-PHEMA)$_p$ micelles were evaluated against HeLa cells by the standard Cell Counting Kit-8 (CCK-8). To perform cytotoxicity assay, HeLa cells were seeded at a density of 5000 cells per well on a 96-well plate and cultured for 24 h. The samples were prepared at a series of desired concentrations. Every experimental well was treated with the samples for 24 h and others were added with fresh medium as control. After 48 h incubation, 10 μL of the CCK-8 stock solution was adder into each well. After incubation for another 1-4 h, the absorbance of each well was measured at a test wavelength of 450 nm. The cell viability of sample was calculated as follow.[35, 39] Data are presented as the average values with standard deviations.

$$\text{Cell viability(\%)} = \frac{\mathrm{A_{test}} - \mathrm{A_{blank}}}{\mathrm{A_{control}} - \mathrm{A_{blank}}} \times 100 \quad (4)$$

where A_{test} and $A_{control}$ represent the intensity determined for cells treated with different samples and for control cells, respectively, and A_{blank} was the absorbance of wells without cells.

2.7 Intracellular release of DOX

Confocal laser scanning microscopy (CLSM) was used to visualize the subcellular localization and intracellular release behavior of DOX-loaded micelles and free DOX for various lengths of time (0.5 h, 4 h and 24 h). First, the HeLa cells were seeded in a glass base dish with a coverslip at a density of 5000 cells and cultured in DMEM supplemented with 10% FBS for 24 h. Then DOX-loaded micelles and free DOX were added, and cells were cultured medium was removed after 0.5 h, 4 h and 24 h at 37°C under 5% CO_2 atmosphere of incubation, and the cells were washed with PBS and stained with DAPI (10 mg L^{-1}) for 0.5 h. Afterwards, the culture medium was replaced with a DMEM medium containing DOX-loaded micelles (0.1 mg L^{-1} of DOX). Finally, the location of intracellular fluorescence was validated using a CLSM imaging system (Zeiss CLSM510) at the excitation wavelength of 480 nm.

2.8 Statistical analysis

All the measurements were performed in triplicate and the data were presented as mean ± standard deviation (n=3).

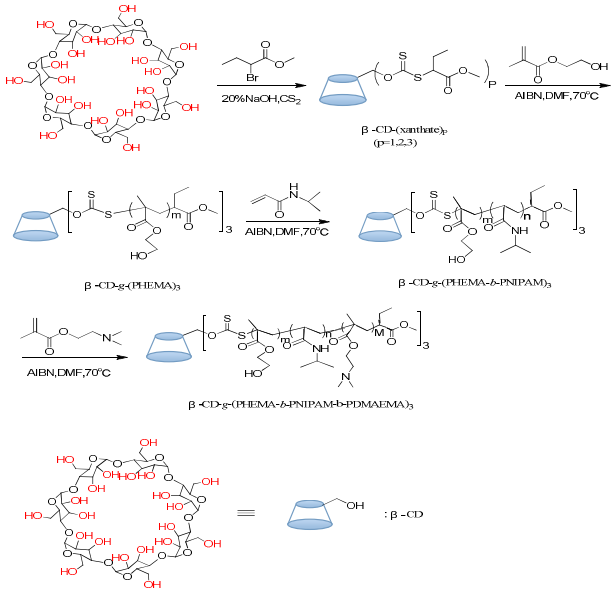

Scheme 1 Synthesis of β-CD-*g*-(PHEMA-*b*-PNIPAM-*b*-PDMAEMA)$_3$ via RAFT using β-CD-based as the macro chain transfer agent.

3. Results and discussion

3.1. Synthesis and Characterization of β-CD-*g*-(PHEMA-*b*-PNIPAM-*b*-PDMAEMA)$_3$

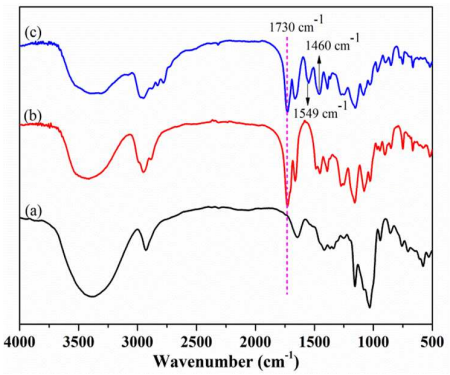

Fig. 1 FTIR spectra of β-CD (a), β-CD-*g*-(PHEMA-*b*-PNIPAM)$_3$ (b), and β-CD-*g*-(PHEMA-*b*-PNIPAM-*b*-PDMAEMA)$_3$ (c).

The β-CD, β-CD-*g*-(PHEMA-*b*-PNIPAM)$_3$ and β-CD-*g*-(PHEMA-*b*-PNIPAM-*b*-PDMAEMA)$_3$ were characterized by FTIR. The structure of β-CD-*g*-(PHEMA-*b*-PNIPAM)$_3$ and β-CD-*g*-(PHEMA-*b*-PNIPAM-*b*-PDMAEMA)$_3$ respectively showed that there was a wide peak round about 1730 cm^{-1} which indicated that the stretch vibration absorption of C-O groups, the peaks at 1549 cm^{-1} was ascribed to N-H bending vibration absorption peak of PNIPAM, the peaks at 1730 cm^{-1} was ascribed to C=O antisymmetric stretching vibration peak of HEMA and PDMAEMA, and the peak at 1460 cm^{-1} was ascribed to -CH_2 stretching vibration peak of and PDMAEMA. In addition, peaks at 1650 cm^{-1}, 1150 cm^{-1} and 1027 cm^{-1} corresponded to C-O, C-O-C glucose units and C-O-C of rings CD were observed.

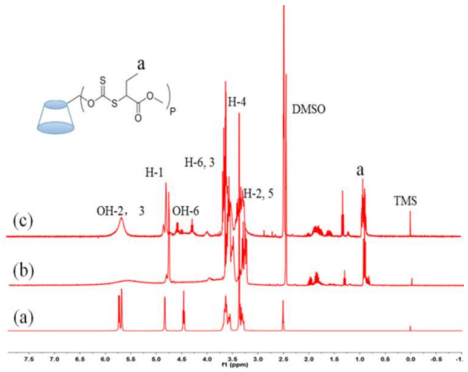

Fig. 2 The ^{1}H NMR spectra of β-CD (a), and β-CD-(xanthate)$_3$ the β-CD/CS_2 molar ratio were1: 3 (b), 1: 1 (c).

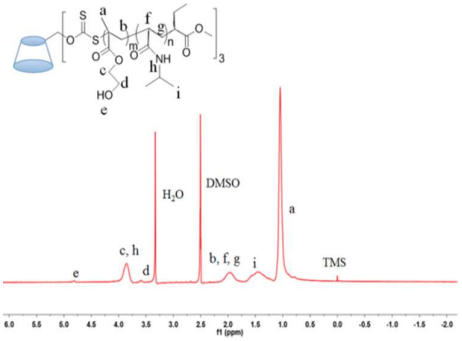

Fig. 3 The ^{1}H NMR spectrum of β-CD-*g*-(PHEMA-*b*-PNIPAM)$_3$.

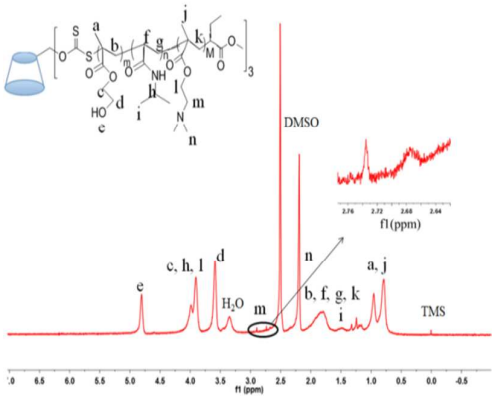

Fig. 4 The ^{1}H NMR spectrum of β-CD-*g*-(PHEMA-*b*-PNIPAM-*b*-PDMAEMA)$_3$.

The chemical structure of β-CD, and β-CD-(xanthate)$_3$ were also characterized by ^{1}H NMR was spectroscopy in DMSO-d_6 (Fig. 2). The signals located at broad chemical shifts in the region of 3.35-3.90 ppm were mainly associated with the inner methylidyne and

methylene protons between the oxygen and carbon moieties (H-4, 5, 6, O-CH-C and O-CH_2-C) on the glucose units of β-CD. The peak located at a chemical shift of δ=4.88 ppm was attributable to the inner methylidyne protons between the oxygen moieties (H-1, O-CHO). The signals located at the chemical shifts in the region of δ=4.19-4.40 ppm were mainly attributable to the hydroxyl protons adjacent to the methylene moieties (OH-6, CH_2-OH). The peak at δ=5.75 ppm corresponds to the hydroxyl protons adjacent to the methylidyne moieties (OH-2，3, CH-OH) of glucose units. In addition, the peak located at a chemical shifts in Fig. 2 (b) and (c) at δ=0.90 ppm was associated with the methyl protons (a, -CH_2CH_3) of the Methyl 2-bromobutyrate groups. However, when the β-CD/CS_2 molar ratio were 1:1 (Fig. 2, (c)), the signals of resonance at δ=5.76 ppm, δ=5.64 ppm, and δ=4.5 ppm were assignable to the protons from the hydroxyl groups of β-CD units and when the β-CD/CS_2 molar ratio was 3:1 (Fig. 2, (b)), the spectrum of the peaks δ=5.64-5.76 and δ=4.43 ppm from the hydroxyl groups of pristine β-CD were showed disappearance completely. Hence, β-CD-(xanthate)$_3$ as the macro-RAFT agent were successfully synthesized and characterized.

Fig. 3 and Fig. 4 shown a comparison of ^{1}H NMR spectra of β-CD-*g*-(PHEMA-*b*-PNIPAM)$_3$ and β-CD-*g*-(PHEMA-*b*-PNIPAM-*b*-PDMAEMA)3 with peak assignments in DMSO-d_6. In Fig. 3 and Fig. 4, the peaks at δ=0.70～1.10 ppm (a, C(CH_3)(COOCH_2CH_2OH), δ=3.58 ppm (d, COOCH_2CH_2OH), and δ=3.89 ppm (c, COOCH_2CH_2OH) were methy and methylene peaks of PHEMA, respectively. Moreover, the peak of δ=4.80 ppm (e, -COOCH_2CH_2OH), was at the end of the hydroxyl chemical shift value of PHEMA. The peak of of methine group (i, -NH-CH(CH_3)$_2$) shifts about δ=1.5 ppm in PNIPAM. The methylene protons neighboring to the carbonyl groups (n, O=C-CH_2) were observed at about δ=2.23 ppm. The peak of methylene protons neighboring to oxygen atoms (c, h, CH_2-O) at δ=4.06 ppm were partly overlapped with that of methine ones in PHEMA and PNIPAM block. The protons of -CH_2N- and -CH_3 of PDMAEMA block were corresponding to the peaks m and j at about δ=2.60 ppm and δ=0.91 ppm, furthermore, the overlapped signals at δ=4.07 ppm, 2.32 ppm, and δ=1.81 ppm belong to the protons of (l, -COOCH_2CH_2-), (n, -N(CH_3)$_2$) and (k, -COOCH_2CH_2-) in PDMAEMA block. Therefore, dual pH and temperature responsive tri-block copolymer β-CD-*g*-(PHEMA-*b*-PNIPAM-*b*-PDMAEMA)$_3$ were successfully synthesized by RAFT polymerization with β-CD-(xanthate)$_3$ as macro-RAFT agent.

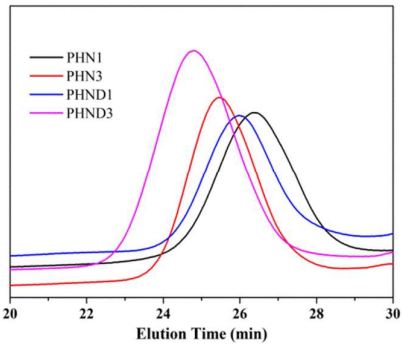

Fig. 5 Evolution of GPC chromatograms of β-CD-*g*-(PHEMA-*b*-PNIPAM)$_P$ and β-CD-*g*-(PHEMA-*b*-PNIPAM-*b*-PDMAEMA)$_P$ copolymers with different molecular weights.

Table 1 Characterization results of the star-shaped and linear block copolymers.

Samples	$M_{n,\,th}$[a]	$M_{n,\,GPC}$[b]	$M_{n,\,NMR}$[c]	PDI[b]
β-CD-*g*-(PHEMA$_{15}$-*b*-PNIPAM$_{34}$)$_1$	6934	7950	8000	1.19
β-CD-*g*-(PHEMA$_{20}$-*b*-PNIPAM$_{45}$)$_3$	24220	22841	23000	1.08
β-CD-*g*-(PHEMA$_{15}$-*b*-PNIPAM$_{34}$-*b*-PDMAEMA$_{78}$)$_1$	19195	20240	20500	1.06
β-CD-*g*-(PHEMA$_{20}$-*b*-PNIPAM$_{45}$-*b*-PDMAEMA$_{63}$)$_3$	34125	32795	33700	1.10

[a]$M_{n,\,th}$ was calculated by theory analysis from the feed ratio of monomers to initiator;
[b]$M_{n,\,GPC}$ was determined by GPC analysis with PS standard, and DMF was used as eluent;
[c]Calculated from ^{1}H NMR data.

3. 2 Formation and Characterization of the blank and DOX-loaded β-CD-*g*-(PHEMA-*b*-PNIPAM-*b*-PDMAEMA) (PHND1 and PHND3) star-shaped triblock copolymer micelles

As an amphiphilic triblock copolymers, when the concentration was above the critical micelle concentration (CMC), β-CD-*g*-(PHEMA-*b*-PNIPAM-*b*-PDMAEMA) could self-assemble into micelles in selective solvent. The hydrophilic PHEMA-*b*-PNIPAM-*b*-PDMAEMA arm chains were mainly in the corona of the micelles, whereas the hydrophobic β-CD chains in the star-shaped triblock copolymer were mainly in the core of the micelles. The hydrophobic of β-CD as cores have been extensively used for drug delivery system. DOX was physically incorporated into PHND1 and PHND3 micelles, which were named D-PHND1 and D-PHND3. The physico-chemical properties of the blank and DOX-loaded micelles were

characterized by DLS analysis, respectively. The average particle sizes, zeta potentials, polydispersity index (PDI) of the blank and DOX-loaded micelles were summarized in Table 2.

Table 2 Hydrodynamic diameter (D_h), size distributions (PDI) and Zeta potentials of blank and DOX-loaaded β-CD-*g*-(PHEMA-*b*-PNIPAM-*b*-PDMAEMA) micelles.

	Blank			DOX-load				
Micelle	$D_{h\,(nm)}$	PDI	Zeta (mV)	$D_{h\,(nm)}$	PDI	Zeta (mV)	DLC (wt%)	DLE (wt%)
PHND1	82.5	0.224	22.59	96.7	0.372	2.78	4.69	46.9 %
PHND3	99.8	0.279	26.74	126.1	0.258	5.68	5.17	51.7 %

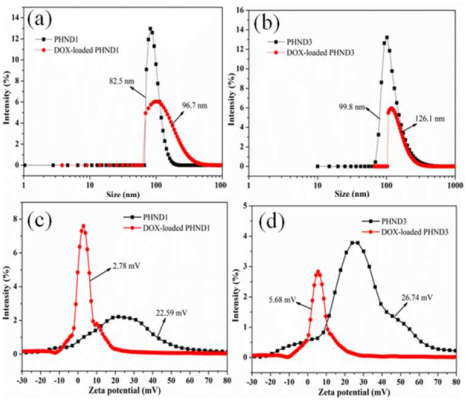

Fig. 6 The particle size distribution curves corresponding to the samples in PHND1 and D-PHND1 (a), PHND3 and D-PHND3 (b) and Zeta potentials of DOX-loaded polymeric micelles in PHND1 and D-PHND1 (c), PHND3 and D-PHND3 (d).

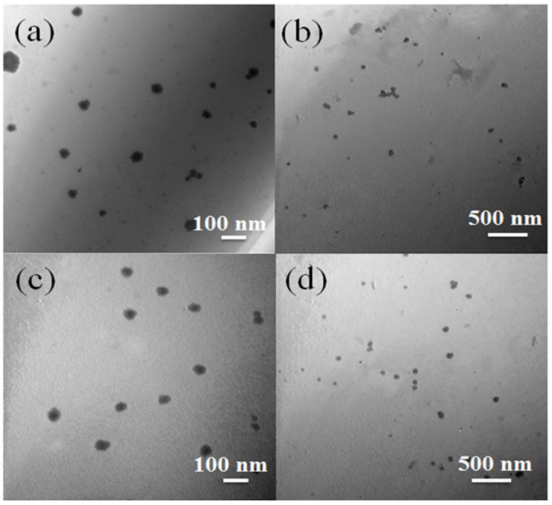

Fig.7 TEM images of for β-CD-*g*-(PHEMA-*b*-PNIPAM-*b*-PDMAEMA)$_1$ (a, b) and β-CD-*g*-(PHEMA-*b*-PNIPAM-*b*-PDMAEMA)$_3$ (c, d) polymeric micelles at 30°C.

As shown in Fig. 6. The hydrodynamic particle size, particle size distribution, polydispersity index (PDI) of the β-CD-*g*-(PHEMA-*b*-PNIPAM-*b*-PDMAEMA) polymeric micelles were evaluated by dynamic light scattering (DLS) and transmission electron microscopy (TEM). The combination of TEM and DLS results confirmed that showed a spherical morphology with the respective average radii around 82.5 and 99.8 nm, respectively (Fig. 7, and Table 2). Fig. 7 indicated that TEM images obtained from aqueous solutions of β-CD-*g*-(PHEMA-*b*-PNIPAM-*b*-PDMAEMA) (PHND1 and PHND3). It was strange that, the self-assembly aggregates of β-CD-*g*-(PHEMA-*b*-PNIPAM-*b*-PDMAEMA) were small spherical. For all the samples (PHND1, a-b and PHND3, c-d), the spherica of polymeric micelles formed at room temperature (30°C). A close view of the enlarged spherical in Fig. 7 showed that some β-CD aggregates connected to each other, tending to a layered irregular structure. According to this observation, we believed that the capability of the β-CD aggregates to form layered crystal were the main driving force in the formation of spherical. At room temperature, the micelles were relatively diameter of about 100 nm in Fig. 7 (a and c, bar=100 nm, b and d, bar=500 nm). As a comparison, the values increased drastically to approximately 600 nm. The change tendency of diameter values of the micelles were consistent with DLS results, however, the diameter of the ellipsoid measured by DLS were larger than that in TEM images, these were due to the DLS results directly reflected the dimension of micelles in solution, where the PHEMA-*b*-PNIPAM-*b*-PDMAEMA chains as the corona were highly stretched in aqueous solution. And we sum up the self-assembly process of β-CD-*g*-(PHEMA-*b*-PNIPAM-*b*-PDMAEMA) in Scheme 2.

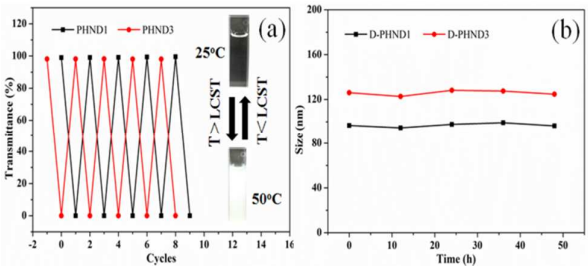

Fig. 8 Plots of transmittance as a function of temperature for β-CD-*g*-(PHEMA-*b*-PNIPAM-*b*-PDMAEMA) copolymer micelle solution (a), particle size of the DOX-loaded polymeric micelles in water at room temperature (b).

As shown in Fig. 8, a stability assay in terms of transmittance and particle size of the β-CD-*g*-(PHEMA-*b*-PNIPAM-*b*-PDMAEMA) polymeric micelles were investigated in water for (a) and (b). The β-CD-*g*-(PHEMA-*b*-PNIPAM-*b*-PDMAEMA) (PHND1 and PHND3) (a) micelles solution was presented reversible transformation of transparency and turbidity during the reversible heating and cooling cycles. It's worth noting that, the phase transition of the micelles were reversible, which showed that the β-CD-*g*-(PHEMA-*b*-PNIPAM-*b*-PDMAEMA) copolymers micelles solution were stable and could undertake a reversible change of swelling and collapse. As shown in Fig. 8 (b), the particle size of the D-PHND1 and D-PHND3 polymeric micelles in water, no apparent change of the particle size. This was indicated that the polymeric micelles have a well long-term stability without the presence of precipitation and phase separation. The results demonstrated that the PHND1 and PHND3 micelles could potentially be used in efficient drug delivery.

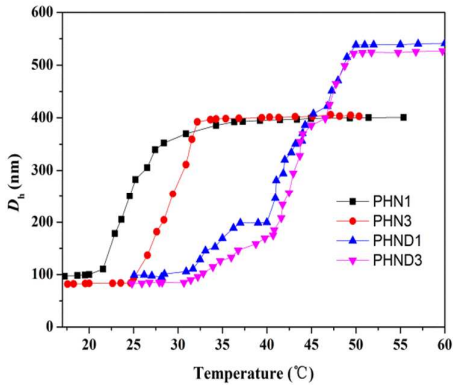

Fig. 9 Effect of temperature on the hydrodynamic radium (D_h) of the micelles of β-CD-(PHEMA-*b*-PNIPAM) (PHN1 and PHN3) and β-CD-*g*-(PHEMA-*b*-PNIPAM-*b*-PDMAEMA)$_3$ (PHND1 and PHND3) in aqueous solution measured at 1 mg mL^{-1}.

As shown in Fig. 9 the plots of the hydrodynamic diameters (D_h) of PHN1, PHN3, PHND1, and PHND3 in water as a function of temperature. When the temperature were relatively lower, the D_h values were small the change slightly. On the contrary, the values were increased significantly in the higher temperature ranges due to the aggregation among micelles. For instance, the D_h value of β-CD-*g*-(PHEMA-*b*-PNIPAM-*b*-PDMAEMA)$_3$ (PHND3) was about 105 nm at 37°C, and the D_h value increased significantly to 300 nm when temperature was raised to 42°C. The schematic process of micelles aggregation with the increase of temperature was shown in Fig. 9. At low temperature range, the PHEMA-*b*-PNIPAM-*b*-PDMAEMA chains existed in random coil conformation owing to the hydrogen-bonding interaction between the triblock copolymers and the water molecules. When the temperature increased to a critical value, PHEMA-*b*-PNIPAM-*b*-PDMAEMA chains will shrink into a spherical structure since the hydrogen bonds between the ether oxygen of PHEMA-*b*-PNIPAM-*b*-PDMAEMA and water molecules collapsed and become hydrophobic. Therefore, the intermolecular hydrophobic attractions were thermodynamically favored and the micelles aggregation will be occured, which resulted in the increase in D_h and visible turbidity.

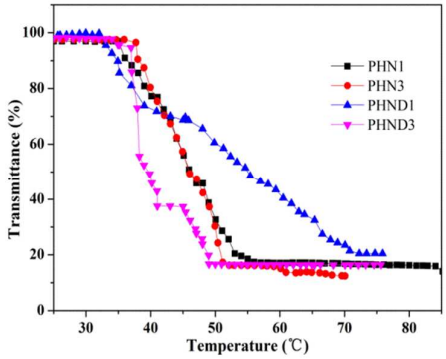

Fig. 10 Transmittance versus temperature for 1 mg mL^{-1} β-CD-g-(PHEMA-*b*-PNIPAM) (PHN1 and PHN3) and β-CD-*g*-(PHEMA-*b*-PNIPAM-*b*-PDMAEMA) (PHND1 and PHND3) aqueous solution at the wavelength of 590 nm and the optical photographs of polymeric aqueous solution at different temperature values.

Dual pH and Thermo-responsive polymers were completely miscible in the solvent in all proportions at temperature below the LCST but tend to collapse and become insoluble above the LCST. The obtained four samples of β-CD-*g*-(PHEMA-*b*-PNIPAM-*b*-PDMAEMA)$_3$ were used to self-assemble into micelles in aqueous solution and the tunable thermo-responsive property was surveyed. Fig. 10 showed the transmittance curves of polymeric micelles in water with different block copolymer. It could be seen that the transmittance curves showed sharp transition during heating process. The LCST values were 32, 37, 31 and 36°C, and its corresponding particle size also were increased from 80 nm to 600 nm in Fig. 8. For the aqueous dispersion of the PHND3 nanoparticles, two separate LCSTs were clearly observed. The transmittance starts to decrease at 36°C, with a middle point at 41°C, corresponding to the first LCST of the PNIPAM block, and it further decreases at 45°C, with a middle point at 49°C, corresponding to the second LCST of the PDMAEMA block. A further increase in the temperature leads to the precipitation of the triblock copolymer nano-particles. The reason was possibly due to the steric repulsion among the crowded PHEMA, PNIPAM and PDMAEMA chains tethered on the β-CD core of the triblock copolymer nanoparticles.

3. 3 Cytotoxicity test

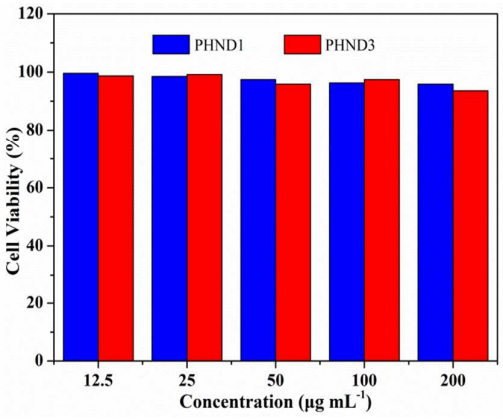

Fig. 11 In vitro cell viability of the β-CD-*g*-(PHEMA-*b*-PNIPAM-*b*-PDMAEMA)$_3$ micelles. Concentration-dependent cell viability of HeLa cells treated with the PHND1 and PHND3 (b) after incubation of 48 h.

Fig. 11 showed the in vitro cytotoxicity of β-CD-*g*-(PHEMA-*b*-PNIPAM-*b*-PDMAEMA) (PHND1 and PHND3), against HeLa cells were evaluated by the CCK-8 assays. Fig. 11 showed the cell viabilities of HeLa cells after 48 h incubation with two kinds of block copolymers with different concentrations. Both block copolymers were showed low toxicity against HeLa cells at various concentrations, and the cell viabilities were still higher than 93% even at the concentration up to 200 μg mL^{-1}. The results suggested that the block copolymers micelle were nontoxic and biocompatible, making them suitable for various applications in biomedical fields which were used as a delivery system for anticancer agents, drug carriers, tissue engineering as well as stimuli-responsive materials.

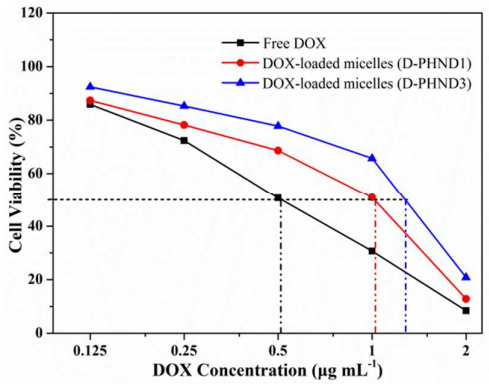

Fig. 12 Cell viability of HeLa cells treated with free DOX and DOX-loaded β-CD-*g*-(PHEMA-*b*-PNIPAM-*b*-PDMAEMA) micelles (D-PHND1, D-PHND3) for 48 h at different concentrations.

The in vitro cytotoxicity of free DOX and DOX-loaded micelles for 48 h against HeLa cells were also investigated by CCK-8 assay. As shown in Fig. 12, DOX-loaded micelles exhibited a slightly lower cytotoxicity to HeLa cells compared with free DOX at the same dosages. These results could be by the prolonged release of DOX from micelles as demonstrated by the in vitro DOX release profile shown in Fig. 12. The IC_{50} values (inhibitory concentration to produce 50% cell death) of DOX-loaded micelles were 0.509 μg mL^{-1}, 1.029 μg mL^{-1}, 1.281 μg mL^{-1}. In contrast, the HeLa cells were incubated with dual pH and temperature responsive block polymeric micelles showed that could be largely caused by the slower release of DOX from the stimuli-responsive polymeric micelles.

3.4 In vitro release of DOX from micelles

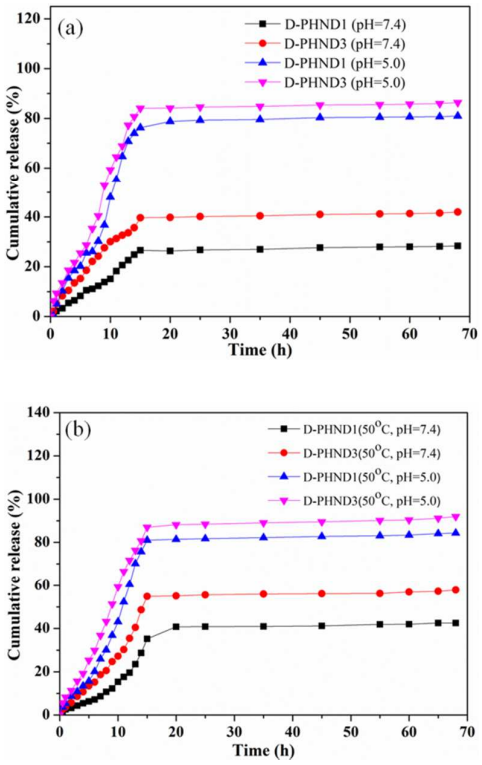

Fig. 13 In vitro release profile of DOX from various DOX-loaded polymeric micelles at 37°C (a) and 50°C (b) under different pH conditions.

The pH-responsive property of the micelles of β-CD-*g*-(PHEMA-*b*-PNIPAM-*b*-PDMAEMA) with block copolymer, the micelles could be used as the pH-controllable drug release carrier. DOX was a kind of hydrophobic anticancer agent and used as the model drug to investigate the controlled property of the micelles. The drug release of the pH-responsive micelles was investigated in PBS (pH 5.0 and 7.4), and the data were shown in Fig. 13. With regard to pH of 7.4 at 37°C, the micelles stayed compact and the loaded DOX were released slowly. After 5 h, less than 20% of DOX (7.44% and 14.72% for D-PHND1 and D-PHND3, respectively) were released. Even after 24 h, only about 26.62% and 39.84% for D-PHND1 and D-PHND3, respectively. In contrast, when the pH was lower at 37°C (pH 5.0), the drug release was accelerated, after 24 h, the cumulative release were 79.28% and 84.46% for D-PHND1 and D-PHND3, respectively.

In addition, when the temperature was raised above the LCST (50°C), the drug release was accelerated owing to the temperature-induced structural changes of the micelles. That was to say, the (PHEMA-*b*-PNIPAM-*b*-PDMAEMA) copolymers shell become hydrophobic, and the micellar core-shell structure was deformed. Therefore, the hydrophobic DOX incorporated in core diffused out quickly from the micelles. Although the mechanism of drug release from polymeric matrices was very complex and was still not completely understood, it could be simplistically classified as either pure diffusion, erosion controlled release or a combination of the two mechanisms [40, 41]. In this study, the results were due to the swollen drug-loaded micelles, attributing to the protonation of amino groups in PDEAEMA segments at weakly acidic conditions. Furthermore, the accelerated micelles rate might be related to the swollen hydrophobic core which could cause the drug molecules close to the surface to diffuse into the medium. Meanwhile, the DOX molecules were not only encapsulated inside the micellar core, but absorbed by the PDMAEMA shell due to the electric action, while only that loaded by hydrophobic effect could be released comparative fast, so it may spend extended period to achieve complete release, which may be concluded from the discussion above. Therefore these results were showed that the copolymer micelles could be had potential applications for the selective release of drugs under intracellular environments. (Scheme 2)

3. 5 In vitro cellular uptake studies

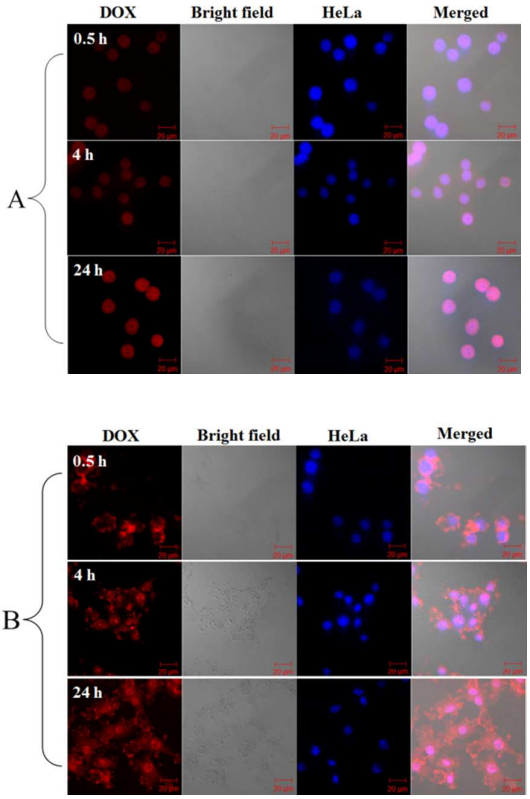

Fig. 14 Comparison of the fluorescence images of HeLa cells incubated with with (A) free DOX and (B) DOX-loaded (D-PHND3) for different times. The dosage of DOX was 5 μg mL^{-1}. For each panel, images from up to down show cell nuclei stained by HeLa (blue), DOX fluorescence in cells (red) and overlays of two images. The scale bars correspond to 20 μm in all the images.

To evaluate the intracellular drug release of β-CD-*g*-(PHEMA-*b*-PNIPAM-*b*-PDMAEMA)$_3$ micelles, the Confocal Laser Scanning Microscopy images was used. The release of DOX from DOX-loaded copolymer micelles could be estimated by observing the red fluorescence intensity of DOX inside the cells. Fig. 14 showed the fluorescence images of HeLa cells were after 0.5, 4 and 24 h of incubation with D-PHND3 using free DOX as a control. One can observed that the fluorescence intensity of DOX became stronger with the increase of incubation time, indicated that DOX was gradually released. Moreover, the fluorescence could be apparently observed at the cytoplasm after 0.5 h incubation (Fig. 14(A)). As shown in Fig. 14(B), DOX was dispersed into the partly cells including nuclei and cytoplasm after 4 and 24 h incubation, more than half of the blue fluorescence was overlapped by red fluorescence and became weaker, it were suggested that DOX was delivered into nuclei and successfully inhibited the proliferation of HeLa cells. While for the DOX-loaded copolymer micelles with much larger sizes, it was likely that the prolonged circulation and passive tumor-targeting delivery process caused by the EPR effect will enhance the delivery of hydrophobic drugs into the tumor cells[3, 42-44], and once the micelles were internalized, it was not easy for them to escape from the cells. In the case of thermo-responsive micelles, as shown in Fig. 14 (B), the intracellular uptake of DOX loaded micelles were showed a much less efficient intracellular release of DOX. The results indicated that free DOX were taken up by diffusion through the cell membrane and the DOX loaded micelles were taken up by the nuclei of cells via the indocytosis process. In addition, the self-assembled micelles of the amphiphilic block copolymers were showed a great potential as anti-tumor drug carriers for cancer therapy.

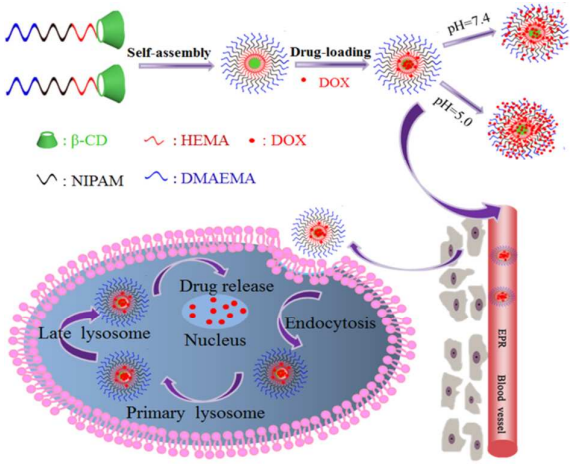

Scheme 2. Illustration of pH-responsive self-assembly of the β-CD-*g*-(PHEMA-*b*-PNIPAM-*b*-PDMAEMA)$_3$ copolymer for the efficient intracellular release of anti-cancer drugs triggered by the acidic microenvironment inside the tumor tissue.

Conclusions

In summary, a novel dual pH and temperature star-shaped triblock copolymer β-CD-*g*-(PHEMA-*b*-PNIPAM-*b*-PDMAEMA)$_3$ has been designed and synthesized by RAFT. These block copolymers could self-assemble into spherical nanoscale micelles comprising of β-CD and HEMA core and (PNIPAM-*b*-PDMAEMA) coronas in aqueous solution. The self-assembly behaviors of the copolymers were investigated by UV-Vis, DLS, and TEM. The LCST of the dual pH and temperature responsive micelles was well controlled 32, 37, 31 and 36^{o}C, the results showed that the copolymers micelles diameters (D_h) were increased from 80 nm to 600 nm in different temperature. The formation of spherical particles micelles and large aggregates were confirmed by TEM and DLS at temperature below and above the LCST, respectively.

The biocompatible block copolymer could self-assemble with the anti-cancer drug DOX into DOX loaded micelles with a size of less than 200 nm. The in vitro release behaviors of DOX from β-CD-*g*-(PHEMA-*b*-PNIPAM-*b*-PDMAEMA)$_3$ micelles exhibited pH-responsive, the release of DOX from the micelles was significantly accelerated by decreasing pH from 7.4 to 5.0 at 37^{o}C, and after 50 h for D-PHND3 micelles, the cumulative release was about 88.7% (w/w), which could be provided sustained drug delivery behavior after the DOX-loaded micelles entered into blood circulation by endocytosis. And the DOX loaded micelles were taken up by the nuclei of cells via the endocytosis process by CLSM. Furthermore, the cytotoxicity tests showed that these star-shaped block copolymers possessed good biocompatibility. The DOX-loaded micelles exhibited a stimuli-responsive release manner, and they could efficiently release DOX into tumor cells and significantly enhance drug efficacy.

Acknowledgements

The authors gratefully acknowledge financial supports from the National Natural Science Foundation of China (21367022) and Bingtuan Innovation Team in Key Areas (2015BD003).

Notes and references

1. Z. Y. Shen, W. Wei , H. Tanaka, K. Kohama, G. H. Ma, T. Dobashi, Y. Maki, H. H. Wang, J. X. Bi and S. Dai, *Pharmacol. Res.*, 2011, **64**, 410-419.
2. T. M. Allen and P. R. Cullis, *Science*, 2004, **303**, 1818-1822.
3. H. R. Wang, J. L. He, M. Z. Zhang, Y. F. Tao, F. Li, K. C. Tam and P. H. Ni, *J. Mater. Chem. B*, 2013, **1**, 6596-6607.
4. C. M.Yu, C. M. Gao, S. Y. Lü, C. Chen, J. L. Yang, X. Di and M. Z. Liu, *Colloid. Surface. B.*, 2014, **115**, 331-339.
5. J. Fang, H. Nakamura and H. Maeda, *Adv. Drug. Deliver. Rev*, 2011,**63**, 136-151.
6. J. Nicolas, S. Mura, D. Brambilla, N. Mackiewicz and P. Couvreur, *Chem. Soc. Rev.*, 2013, **42**, 1147-1235.
7. T. Endres, M. Y. Zheng, A. Kılıç, A. Turowska, M. B. Broichsitter, H. Renz, O. M. Merkel and T. Kissel, *Mol. Pharm.*, 2014, **11**, 1273-1281.
8. W. F Ma, K. Y. Wu, J. Tang, D. Li, C. Wei, J. Guo, S. L. Wang and C. C. Wang, *J. Mater. Chem.*, 2012, **22**, 15206-15214.
9. J. M. Hu, T. Wu, G. Y. Zhang and S. Y. Liu, *J. Am. Chem. Soc.*, 2012, **134**, 7624-7627.
10. S. Mura, J. L. Nicolas and P. Couvreur, *Nat. Mater.*, 2013, **12**, 991-1003.
11. L. A. Fielding, J. A. Lane, M. J. Derry, O. O. Mykhaylyk and S. P. Armes, *J. Am. Chem. Soc.*, 2014, **136**, 5790-5798.
12. P. J. Sun, Y. Zhang, L. Q. Shi and Z. H. Gan, *Macromol. Biosci.*, 2010, **10**, 621-631.
13. W. Agut, A. Brulet, C. Schatz, D. Taton and S. Lecommandoux, *Langmuir*, 2010, **26**, 10546-10554.
14. L. P. Qiu, Z. Li, M. X. Qiao, M. M. Long, M. Y. Wang, X. J. Zhang, C. M. Tian and D. W. Chen, *Acta Biomater.*, 2014, **10**, 2024-2035.
15. Z. Wang, B. H. Tan, H. Hussain and C. He, *Colloid Polym. Sci.*, 2013, **291**, 1803-1815.
16. J. Mao, X. L. Ji and S. Q. Bo, *Macromol. Chem. Phys.*, 2011, **212**, 744-752.
17. Z. R, Guo , Y. J. Feng, D. W. Zhu , S. A. He , H. B. Liu , X. R. Shi, J. Sun and M. Z. Qu, *Adv. Funct. Mater.*, 2013, 23, 5010-5018.
18. N. Hadjichristidis, M. Pitsikalis, S. Pispas and H. Iatrou, *Chem. Rev*, 2001, **101**, 3747-3792.
19. H. J. Kang, Y. Su, X. He, S. F. Zhang, J. Z. Li and W. Q. Zhang, *J. Poly. Sci. Pol. Chem.*, 2015, **53**, 1777-1784.
20. X. H. Wang, S. T. Li, Y. Su, F. Huo and W. Q. Zhang, *J. Poly. Sci. Pol. Chem*, 2013, **51**, 2188-2198.
21. X. H. Wang, J. X. Xu, Y. Y. Zhang and W. Q. Zhang, *J. Poly. Sci. Pol. Chem*, 2012, **50**, 2452-2462.
22. A.M. Master, M. E. Kenney, N. L. Oleinick and A. S. Gupta, *J. Pharm. Sci.*, 2010, **99**, 2386-2398.
23. L. Li, B. B. Lu, J. N.Wu, Q. K. Fan, X. H. Guo and Z. Y. Liu, *New J. Chem*., 2016, 40, 4761-4768.
24. L. Li, B. B. Lu, Q. K. Fan, L. L. Wei, J. N. Wu, J. Hou, X. H. Guo and Z.Y. Liu, *RSC Adv.*, 2016, **6**, 27102-27112.
25. J. C. Chen, M. Z. Liu, H. H. Gong, Y. J. Huang and C. Chen, *J. Phys. Chem. B.*, 2011, **115**, 14947-14955.
26. S. Ohno, H. F. Gao, B. Cusick, T. Kowalewski and K. Matyjaszewski, *Macromol. Chem. Phys.*, 2009, **210**, 421-430.
27. K. Matyjaszewski, P. J. Miller, J. Pyun, G. Kickelbick and S. Diamanti, *Macromolecules*, 1999, **32**, 6526-6535.
28. F. Manakker, T. Vermonden, C. F. Nostrum and W. E. Hennink, *Biomacromolecules*, 2009, **10**, 3157-3175.
29. G. S. Chen and M. Jiang, *Chem. Soc. Rev.*, 2011, **40**, 2254-2266.
30. K. Uekama, F. Hirayama and T. Irie, *Chem. Rev*, 1998, **98**, 2045-2076.
31. R. Machín, J. R. Isasi and I. Vélaz, *Carbohyd. Polym.*, 2012, **87**, 2024-2030.
32. H. J. Zhang, Q. Yan, Y. Kang, L. L. Zhou, H. Zhoua, J. Y. Yuan and S. Z. Wu, *Polymer*, 2012, **53**, 3719-3725.
33. B. Charleux, G. Delaittre, J. Rieger and F. D'Agosto, *Macromolecules*, 2012, **45**, 6753-6765.
34. Q. L. Li, C. Q. Gao, S. T. Li, F. Huo and W. Q. Zhang, *Polym. Chem.*, 2014, **5**, 2961-2972.
35. M. M. Zhang, Q. Q. Xiong, J. Q. Chen, Y. S.Wang and Q. Q. Zhang, *Polym. Chem.*, 2013,**4**, 5086-5096.
36. Y. Zhang, H. F. Chan and K. W. Leong, *Adv. Drug. Deliver. Rev.*, 2013, **65**, 104-120.
37. Y. J. Wang and C. M. Dong, *J. Polym. Sci. Pol. Chem.*, 2012, **50**, 1645-1656.
38. J. L. Guo,Q. X. Zhang,Y. B. Peng, Z. H. Liu, L. Y. Rao,T. He, J. Crommen, P. H. Sun and Z. J. Jiang, *J. Sep. Sci.*, 2013, **36**, 2441-2449.
39. Q. M. Liu, J. Chen and J. Z. Du,. *Biomacromolecules*, 2014, **15**,

3072-3082.
40. Z. S. Ge and S. Y. Liu, *Chem. Soc. Rev.*, 2013, **42**, 7289-7325.
41. G. Y. Li, N. N. Yu, Y. R. Gao, Q. Tao and X. Y. Liu, *Int. J. Biol. Macromol.*, 2016, **82**, 381-386.
42. X. D. Liu, B. Z. Chen, X. J. Li, L. F. Zhang, Y. J. Xu, Z. Liu, Z. P. Cheng and X. L. Zhu, *Nanoscale*, 2015, **7**, 16399-16416.
43. H.H. Kuang, Y. J. Wu, Z. Y. Zhang, J. Z. Li, X. S. Chen, Z. G. Xie, X. B. Jing and Y. B. Huang, *Polym. Chem*., 2015, **6**, 3625-3633.
44. Z. L. Tyrrell, Y. Q. Shen and M. Radosz, *Prog. Polym. Sci*., 2010, **35**, 1128-1143.